photonics

Communication

High-Peak-Power Sub-Nanosecond Mode-Locking Pulses Generated by a Dual-Loss-Modulated QML Laser with AOM and $SnSe_2$

Zihao Dai [1,†], Baohao Xu [1,†], Xinyu Hu [1], Kai Jiang [1], Jing Wang [1], Wenjing Tang [1,*] and Lihua Cao [2]

1 School of Physics and Technology, University of Jinan, Jinan 250022, China; 201831703039@stu.ujn.edu.cn (Z.D.); 202121200764@stu.ujn.edu.cn (B.X.); 202021100171@stu.ujn.edu.cn (X.H.); sps_jiangk@ujn.edu.cn (K.J.); ss_wangj@ujn.edu.cn (J.W.)
2 Engineering Training Center, Shandong University, Jinan 250100, China; caolh89@sdu.edu.cn
* Correspondence: sps_tangwj@ujn.edu.cn
† These authors contributed equally to this work.

Abstract: In order to investigate the pulse modulation potential of $SnSe_2$ in all-solid-state lasers, an active and passive dual-loss-modulated (APDM) Q-switched and mode-locking (QML) Nd:YVO_4 laser was realized by employing an acousto-optic modulator (AOM) and a 5.9 nm thick $SnSe_2$ saturable absorber (SA). The significant pulse compression ability of $SnSe_2$ film was found experimentally, and sub-nanosecond mode-locking pulses with large peak power were obtained. The average output power, pulse energy, and pulse width versus the pump power were measured. With a pump power of 8.5 W, 242 ps mode-locking pulses with a pulse peak power of 231.4 kW were realized successfully. The experimental results also show that the $SnSe_2$-based APDM QML laser has great potential in generating sub-nanosecond pulses with large peak power and high stability.

Keywords: dual-loss-modulated; $SnSe_2$ saturable absorber; QML pulse; high peak power; sub-nanosecond

check for updates

Citation: Dai, Z.; Xu, B.; Hu, X.; Jiang, K.; Wang, J.; Tang, W.; Cao, L. High-Peak-Power Sub-Nanosecond Mode-Locking Pulses Generated by a Dual-Loss-Modulated QML Laser with AOM and $SnSe_2$. *Photonics* **2022**, *9*, 471. https://doi.org/10.3390/photonics9070471

Received: 19 June 2022
Accepted: 4 July 2022
Published: 6 July 2022

1. Introduction

Stable all-solid-state lasers with high peak power and ultrashort pulse width and high pulse stability are expected in many fields, such as nonlinear frequency conversion, precision machining, or medical treatment [1–5]. As we know, the most widely used pulse modulation technologies for all-solid-state lasers are Q-switching and mode-locking. However, because of the large pulse width of Q-switched lasers and high pulse repetition rate of mode-locking lasers, it is difficult to generate ultrashort pulses with high peak power [6–8]. In comparison, the dual-loss modulation Q-switched and mode-locking (QML) technology can remedy this problem. By selecting the appropriate modulator components, a high-quality sub-nanosecond pulse train with high peak power can be produced in an active and passive dual-loss-modulated (APDM) QML laser [9,10].

Currently, two-dimensional (2D) materials are widely used in pulse lasers as saturable absorbing materials [11–15]. For example, 2D tin diselenide ($SnSe_2$) has received widespread interest as an ecologically benign material [16–19]. Furthermore, $SnSe_2$ nanosheets possess an ultrafast recovery time, broadband saturable absorption, and faster carrier mobility and optical response rate, which make it highly suitable for mode-locking lasers as a saturable absorber (SA) [20]. In 2017, the saturable absorption characteristics of $SnSe_2$ nanosheets in solid-state laser were investigated by Cheng et al., and a 129 ns Q-switched pulse was obtained [21]. In 2018, a solid-state passive Q-switched Tm:YAP laser at 2 µm with $SnSe_2$ saturable absorber was presented by Liu et al., and 1.29 µs Q-switched pulses with an output power of 400 mW were achieved [22]. Then, in 2019, a $SnSe_2$-based solid-state passive Q-switched laser at 1.3 and 1.9 µm was reported, which demonstrate the effective optical modulation properties of the $SnSe_2$ [23]. For fiber lasers, the pulse characteristics modulated by the $SnSe_2$-SA were also successfully demonstrated by Q-switched or mode-locked technologies [24–27]. However, in solid-state lasers, studies on the mode-locking pulse modulation characteristics of $SnSe_2$ are not enough. There is no related report on the application of $SnSe_2$-SA in a solid-state APDM QML laser.

According to our previous studies, the Q-switched envelop repetition rate is completely controlled by the active modulator in APDM QML lasers [9,10]. Moreover, compared with the single passive or active modulated QML lasers, in APDM QML laser, the pulse duration of the Q-switched envelop can be greatly reduced, and the amplitude stability can be greatly improved [28]. Furthermore, a shorter Q-switched envelope width results in fewer mode-locking pulses. At the same time, the whole energy of the Q-switched envelope can be confined to these few mode-locking pulses. Thus, high-peak-power mode-locking pulses with high stability can be obtained [29]. Up to now, there is no report about the application of $SnSe_2$ in all-solid-state APDM QML lasers at the wavelength of 1.06 μm.

In this work, using $SnSe_2$-SA and an acousto-optic modulator (AOM), an all-solid-state APDM QML laser was realized successfully. At the maximum pump power of 8.5 W, the Q-switched envelop was greatly compressed to contain only two sub-nanosecond mode-locking pulses. The minimum mode-locking pulse duration of 242 ps was obtained with a peak power of 231.4 kW. To the authors' knowledge, this is the first time that such a system has been reported.

2. Preparation and Characterization of $SnSe_2$-SA

In our work, the $SnSe_2$ nanosheets was fabricated by the liquid-phase exfoliation (LPE) method [29]. The dispersion was obtained from the mixed liquor of 25 mg $SnSe_2$ power and 10 mL of absolute ethyl alcohol by sonication and centrifugation. Then, a 10 μL $SnSe_2$ dispersion was dripped onto a 20 mm × 20 mm × 1 mm sapphire substrate using spin-coating technology. Here, the spin-coating speed was 300 rpm. The sapphire substrates we used were polished on both sides without coating. After drying, the high-quality $SnSe_2$-SA was prepared.

In order to characterize the performance of the $SnSe_2$ film, the stereoscopic scanning electron microscopy (SEM) image was first obtained (Figure 1a) to show the clear layered structure. As shown in the SEM image, the edge of the $SnSe_2$ deposition can be clearly observed. The Raman spectrum was recorded by a Raman spectrometer (LabRAM HR Evolution UV-Vis-NIR, Horiba, Paris, France). Figure 1b shows the main E_g mode (107.2 cm^{-1}) and A_{1g} mode (181.3 cm^{-1}) of the $SnSe_2$ film sample. For $SnSe_2$, it has been found that the Raman shift could be linked to the thickness of $SnSe_2$ nanosheets. The frequencies of the E_g mode and the A_{1g} mode decreased monotonically as the thickness changed from the bulk (115.5 cm^{-1} and 188.3 cm^{-1}) down to a monolayer [18,30]. For our $SnSe_2$ nanosheet sample, frequencies of E_g mode and the A_{1g} mode were all significantly smaller than that of the bulk. The atomic force microscopy (AFM) showed the morphology and thickness of $SnSe_2$ film in Figure 1c,d; the corresponding average thickness of the $SnSe_2$ film sample was about ~5.9 nm. Assuming that the monolayer flake thickness was 0.6 nm, the saturable absorber we made had about 9–10 layers [25]. The $SnSe_2$ flake sample also had a large lateral dimension of about ~2 μm.

The nonlinear transmission curve was fitted according to the experimental values (Figure 2). A 78 ns solid-state Q-switched laser at 1.06 μm wavelength was constructed as the test light source. In our opinion, the saturable absorption of the $SnSe_2$-SA sample near 1 μm was mainly caused by the edge energy levels and atomic vacancy defect energy levels [31–33]. By fitting the experimental data, an approximated initial transmittance (T_0) of 72% could be obtained. When the saturable absorber was saturated, the saturated transmittance (T_{sat}) was fitted to be about 76.42%. The modulation depth ΔT, saturation intensity I_{sat}, and non-saturated absorption rate T_{ns} were determined to be 4.4%, 17.23 MW/cm^2, and 23.54%, respectively.

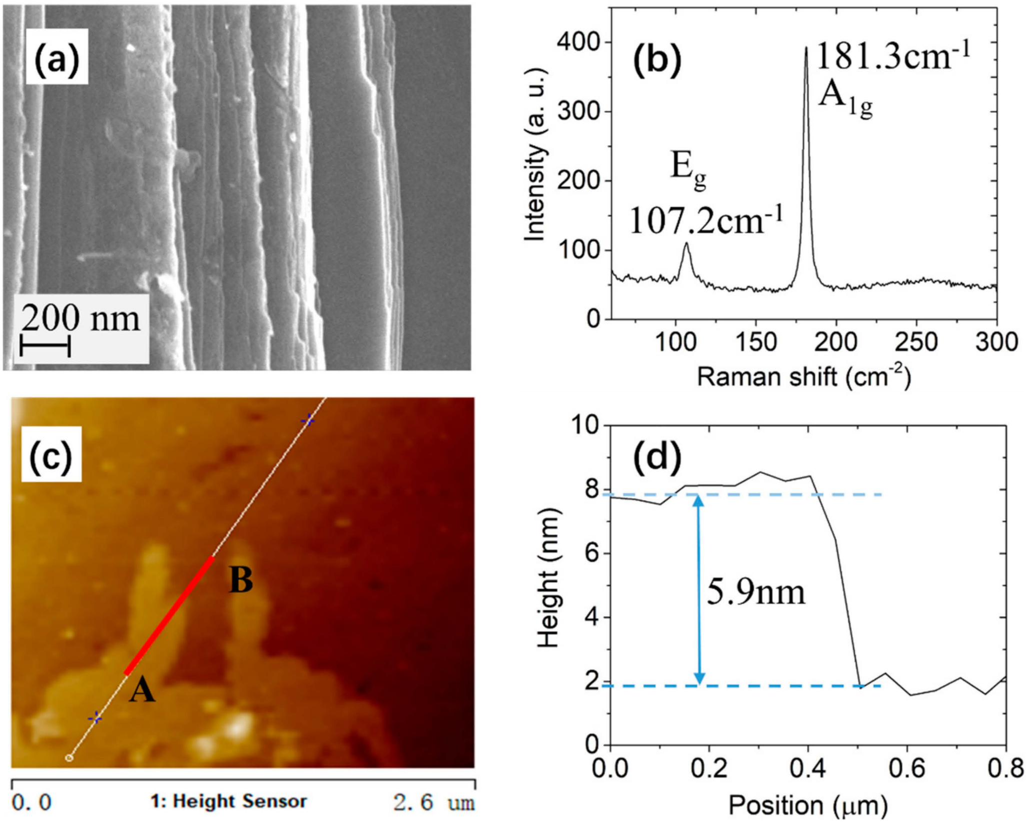

Figure 1. (**a**) SEM image; (**b**) Raman spectrum; (**c**) AFM image; (**d**) corresponding height curve.

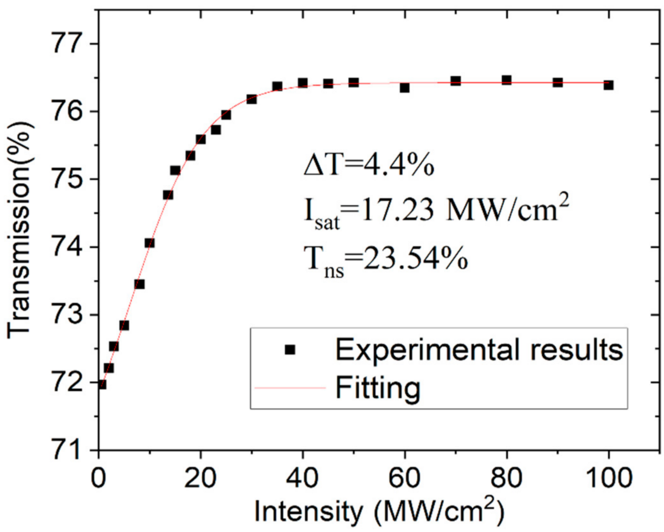

Figure 2. Nonlinear transmittance curve of the $SnSe_2$ film.

3. Experimental Setup and Results

3.1. Experimental Setup

Figure 3 exhibits the setup of the APDM QML laser modulated by AOM and $SnSe_2$-SA. A four-mirror resonator with a cavity length of 141.5 cm was set up. Plane mirrors M1 and M4 acted as the input mirror and output mirror, respectively. Spherical concave mirrors M3 (ROC = 500 mm) and M4 (ROC = 150 mm) both had a high-reflection coating at 1064 nm. The transmittance of the output coupling mirror M4 was 15%. An optical coupling system was used to couple the pump light from the pump source into the laser crystal. The pump source emitting at 808 nm was a fiber-coupled diode laser with a beam diameter of 400 μm and maximum output power of 20 W. A 3 × 3 × 8 mm^3 Nd:YVO$_4$ crystal (0.5 at.%) was selected as the laser medium to achieve laser amplification at 1064 nm. As one of the most excellent laser media for diode-pumped solid-state lasers, the Nd:YVO$_4$ crystal features large emission cross-sections, as well as high environmental stability, which are beneficial to generate high peak power and narrow pulse width [9,34]. Furthermore, the cross-sectional size of 3 × 3 mm^2 and the doping concentration of 0.5 at.% were conducive to the heat dissipation, reducing the thermal effect of the Nd:YVO$_4$ crystal and resulting in a better laser characteristics [35]. An AOM with a 45 mm long quartz crystal was used as the active modulator. The entire experiment was carried out at a room temperature of 25 °C. Both the Nd:YVO$_4$ and the AOM crystals were maintained at 18 °C by a water chiller to mitigate thermal effects. The SnSe$_2$-SA was placed at a tight focusing position near M4 to provide steady and effective mode-locking. According to the ABCD matrix, the average beam waist radius at the position of the absorber was about 113 µm. A photoelectronic diode and a TDS620B digital oscilloscope (Tektronix, Beaverton, OR, USA) were used to record the pulse temporal behavior.

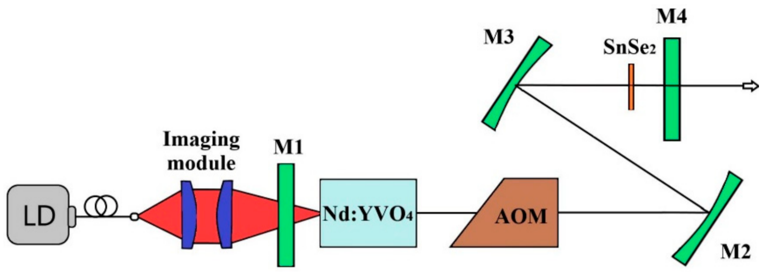

Figure 3. The setup of the APDM QML laser.

3.2. Experimental Results and Discussion

The output performances of APDM QML Nd:YVO$_4$ laser with AOM/SnSe$_2$ were investigated by experiment. The pulse performances versus the AOM frequencies *f* and the pump power were recorded. Furthermore, for comparison, the performance of a single QML Nd:YVO$_4$ laser with SnSe$_2$-SA was also investigated by moving the AOM out of the cavity. For each pump power value, the average output power and pulse shape were measured sequentially by the power meter and oscilloscope. As the pump power increased, the laser was always in a stable QML state.

Figure 4 shows the variation curves of the average output powers of SnSe$_2$ single QML and AOM/SnSe$_2$ APDM QML lasers. The average output power increased monotonically with increasing pump power. Under the pump power of 8.5 W, the average output powers of 561, 710, and 889 mW were obtained from the AOM/SnSe$_2$ APDM QML laser under f = 5, 10, and 15 kHz, respectively. Moreover, 651.2 mW power could be obtained for the single passive QML laser with SnSe$_2$-SA. By fitting, the slope efficiencies of 11%, 9.3%, 12%, and 15.1% could be obtained for SnSe$_2$ single and AOM/SnSe$_2$ APDM QML lasers at f = 5, 10, and 15 kHz, respectively. Obviously, a larger modulation frequency could produce a higher average output power.

For further analysis of the pulse energy, the repetition rates of Q-switched envelopes in the SnSe$_2$ single QML laser were also recorded. Within the pump range of 2.5 W to 8.5 W, the repetition rates of the Q-switched envelopes increased from 26 kHz to 225 kHz. Combining the pulse repetition rates and average output power, the single envelope energies could be calculated as depicted in Figure 5. Under the pump power of 8.5 W, single envelope energies of 112, 71, and 59.2 µJ could be obtained from APDM QML lasers with AOM/SnSe$_2$ for f = 5, 10, and 15 kHz, respectively. However, in the single QML laser with SnSe$_2$, only 2.9 µJ single envelope energy could be achieved. The maximum single envelope energy obtained by the APDM QML laser was about ~39 times as large as that of the single QML laser. This was mainly due to the lower pulse repetition rate produced by the APDM QML laser.

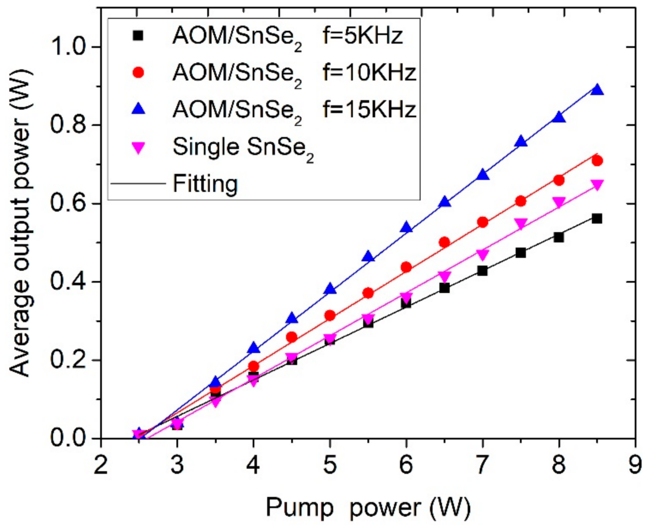

Figure 4. The variation curves of average output power for QML lasers with different modulation methods.

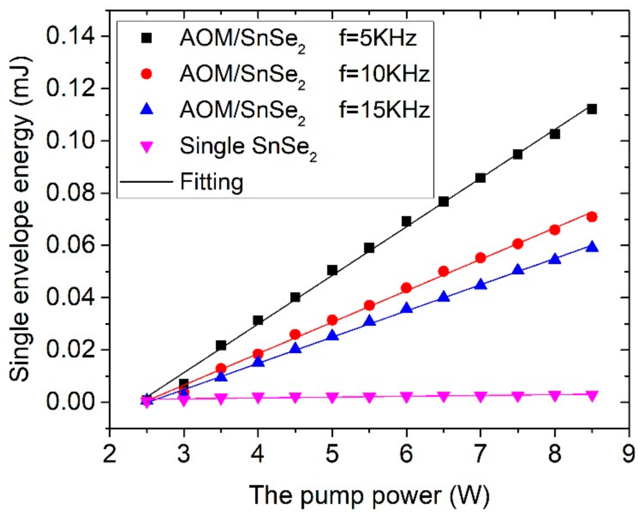

Figure 5. Variation of the single envelope energy with the pump power for QML lasers with different modulation methods.

Figure 6 shows the variation of the envelope width with the pump power. For QML lasers with $SnSe_2$, the shortest Q-switched envelope duration of 291 ns was obtained at 8.5 W pump power. However, the APDM mechanism could greatly reduce the envelope width. The shortest Q-switched pulse envelope durations of 18, 34, and 52 ns were obtained in APDM QML lasers with AOM/$SnSe_2$ at f = 5, 10, and 15 kHz, respectively, which were much narrower than that of the single QML laser. The maximum compression ratio of the Q-switched envelope duration was approximated to be 93.8% from 291 ns (in $SnSe_2$ QML laser) to 18 ns (in AOM/$SnSe_2$ QML laser).

Furthermore, the number of mode-locked pulses in the envelope decreased significantly as the width of the envelope decreased. The temporal shapes of QML pulses under the pump power of 8.5 W were recorded (Figure 7). Figure 7a shows the temporal profiles of single Q-switched envelope and single mode-locked pulse in QML laser with single $SnSe_2$. The single mode-locked pulse width displayed by the oscilloscope was 760 ps. For APDM QML laser, the number of mode-locking pulses in one envelope decreased to only a few with decreasing pulse repetition rate. The corresponding temporal profiles for different modulation frequencies are exhibited in Figure 7b–d. As shown in the figures, there were only two, three, and five mode-locking pulses in one envelope for f = 5, 10, and 15 kHz, respectively. The corresponding pulse widths of single mode-locked pulses displayed by the oscilloscope were 544, 591, and 620 ps, respectively.

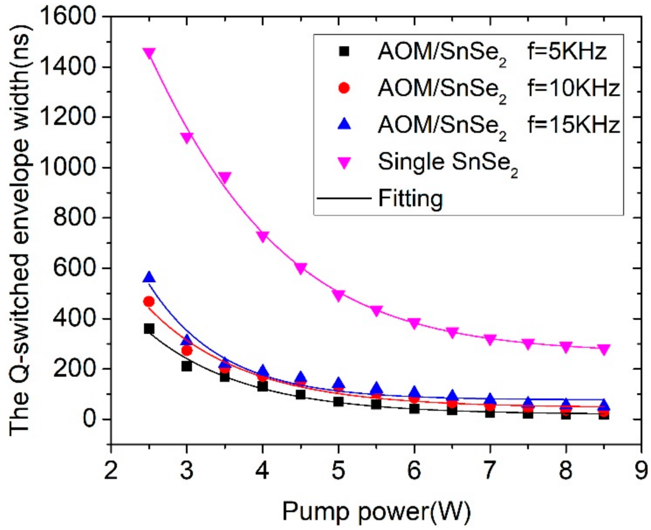

Figure 6. The variation of Q-switched envelope width for QML lasers with different modulation methods.

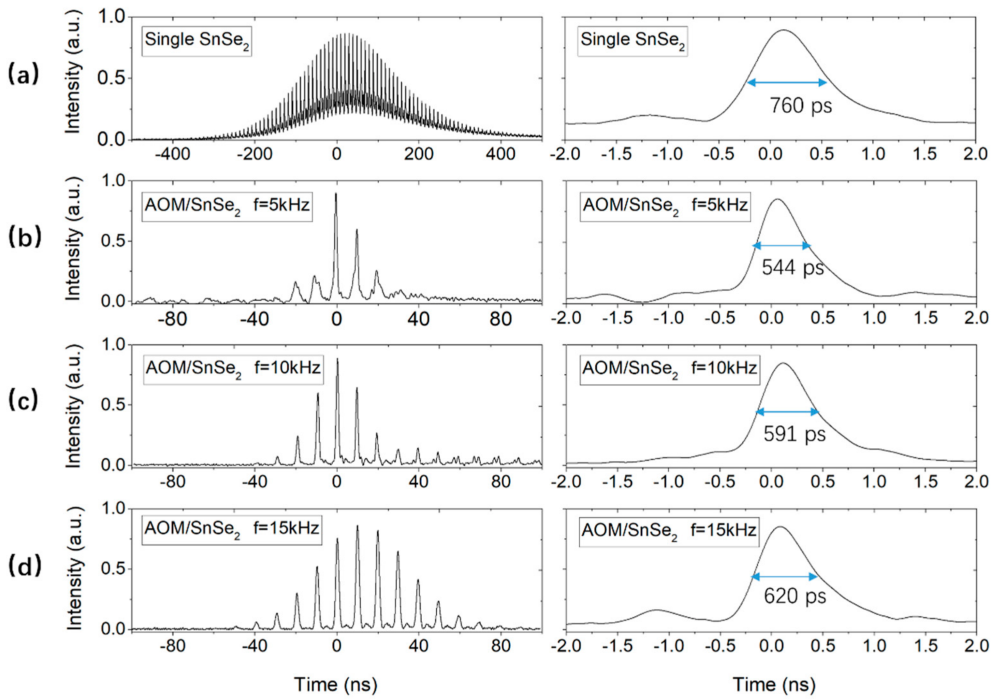

Figure 7. The temporal shapes of QML pulse envelope and single mode-locking pulses with different modulation methods at the pump power of 8.5 W: (**a**) single QML laser with $SnSe_2$; (**b**) APDM OML laser with f = 5 kHz; (**c**) APDM OML laser with f = 10 kHz; (**d**) APDM OML laser with f = 15 kHz.

Because the response time of the digital oscilloscope we used was 350 ps, which was comparable with the rise time and the fall time of the mode-locking pulse, the pulse width values read by the oscilloscope were not accurate. Combining the user manual of oscilloscope and the estimated formula $t_{est} = 1.25\sqrt{t_{measure}^2 - t_{osc}^2 - t_{pro}^2}$, the pulse widths could be estimated by the extended pulse shapes shown in Figure 7 [9,28,36–38]. Here, t_{est} is the estimated pulse duration of the mode-locking pulse, $t_{measure}$ is the measured rise time of the mode-locking pulse from oscilloscope, t_{pro} is the rise time of the probe, and t_{osc} is the rise time of the oscilloscope. In our experiment, the rise times of the oscilloscope and probe were 350 ps and 14 ps, respectively. When the pump power reached 8.5 W, the shortest estimated mode-locking pulse durations obtained were 546 ps for the single QML laser and 242, 410, and 463 ps for the APDM OML laser with f = 5, 10, and 15 kHz, respectively. The calculated results were much shorter than the measured values.

In order to further investigate the dual-loss modulation mechanism, as a comparison, the time-domain characteristics of single AOM modulated lasers were also recorded. When removing the $SnSe_2$-SA, the lasers still operated in the QML state with AOM. However, the pulse widths of the Q-switched envelopes and mode-locking pulses were much larger than those of the APDM QML laser. At the pump power of 8.5 W and f = 5 kHz, the shortest Q-switched envelope pulse duration of 92 ns could be obtained from the actively QML laser with AOM, corresponding to a 1.82 ns pulse duration of a mode-locking pulse underneath the Q-switched envelope. Obviously, it can be concluded that the $SnSe_2$-SA played a significant role in compressing the pulse width of the Q-switched envelope and mode-locking pulse in the APDM QML laser.

Combining the single envelope energies and the number of mode-locking pulses in a single envelope, the mode-locking pulse peak power of the APDM QML laser could be calculated. Under the maximum pump power of 8.5 W, the maximum peak powers of mode-locking pulses were 231.4, 57.7, and 25.6 kW for f = 5, 10, and 15 kHz, respectively. In the APDM QML laser, the pulse peak powers with low repetition rate were improved significantly. This is also one of the advantages of the APDM mechanism.

The stability of the pulse is also a key factor in measuring the quality of the laser. During the experiment, the oscilloscope shapes of the pulse envelope sequence were recorded after the lasers were running continuously for 6 h. Figure 8 gives the envelope sequence shapes. The standard deviations of pulse envelope sequence amplitudes were calculated. Under 8.5 W pump power and 5 kHz modulated frequency, the amplitude root-mean-square error (RMSE) of the APDM lasers with $SnSe_2$/AOM was 0.00255, which is much smaller than the 0.04592 RMSE of the single $SnSe_2$-SA QML laser. Obviously, the APDM QML laser's stability was clearly superior to that of the $SnSe_2$-based passive QML laser, which can be seen very intuitively through the figure. This also shows that the APDM method had a significant effect on the improvement of pulse stability. The long-term stability of the laser system was also investigated; a stable QML operation of the APDM QML laser was maintained for at least 6 h every day for 1 week.

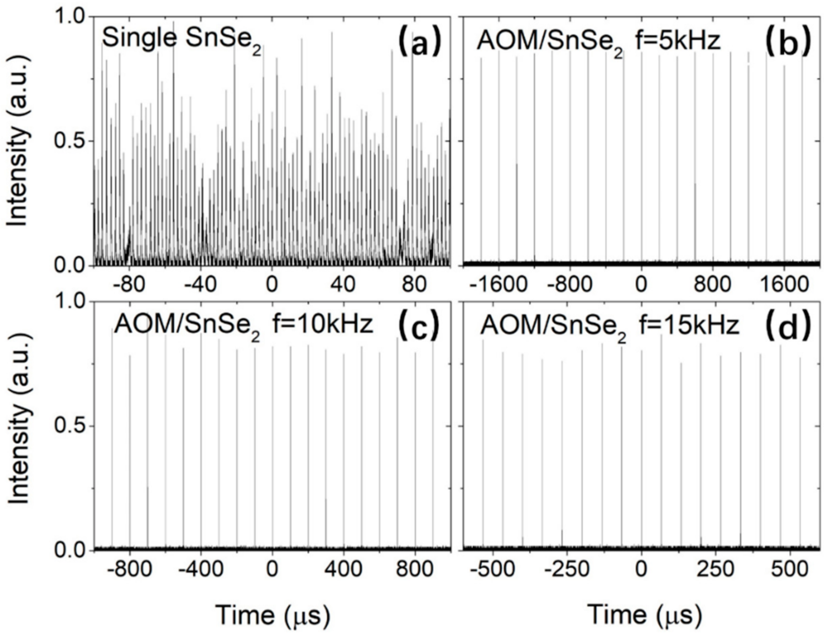

Figure 8. Oscilloscope shapes of the envelope sequences at 8.5 W pump power: (**a**) single $SnSe_2$-SA QML; (**b**) $SnSe_2$/AOM APDM QML with f = 5 kHz; (**c**) $SnSe_2$/AOM APDM QML with f = 10 kHz; (**d**) $SnSe_2$/AOM APDM QML with f = 15 kHz.

In order to further demonstrate the robustness of the APDM QML system, by employing the 90.0/10.0 scanning-knife-edge method, the beam profile characteristics for the high-peak-power sub-nanosecond APDM QML laser were measured. The beam quality factors (M^2) in the horizontal and longitudinal planes were 1.86/1.53, which were hardly changed by the different modulation frequencies *f*.

4. Conclusions

To sum up, a diode-pumped APDM QML laser with sub-nanosecond pulse width was realized using an AOM and $SnSe_2$ film. Under a maximum pump power of 8.5 W, a pulse peak power of 231.4 kW with a pulse duration of 242 ps was obtained. The study results of this work show that the APDM QML technology based on $SnSe_2$-SA is an economical way to produce stable sub-nanosecond pulses with large peak power. Moreover, in this type of laser, a lower modulation frequency of AOM is beneficial for higher stability, narrower pulse width, and larger peak power.

Author Contributions: Z.D. and B.X. designed and performed the experiments, analyzed the data, and drafted the manuscript; X.H. and K.J. fabricated and characterized the saturable absorber; J.W. and W.T. performed the theoretical analysis; L.C. provided some experimental equipment; all authors contributed to editing the manuscript. All authors have read and agreed to the published version of the manuscript.

Funding: This research was funded by the National Natural Science Foundation of China, grant number 62005094, the Program of Jinan Introduced Innovation Team, grant number 2018GXRC011, the Natural Science Foundation of Shandong Province, grant number ZR2021MF128, and the Doctoral Fund Project from University of Jinan, grant number XBS1917.

Institutional Review Board Statement: Not applicable.

Informed Consent Statement: Not applicable.

Conflicts of Interest: The authors declare no conflict of interest.

References

1. Peng, Q.J.; Zong, N.; Zhang, S.J.; Wang, Z.M.; Yang, F.; Zhang, F.F.; Zhou, X.J. DUV/VUV all-solid-state lasers: Twenty years of progress and the future. *IEEE J. Sel. Top. Quantum Electron.* **2018**, *24*, 1602312. [CrossRef]
2. Steiner, R. New laser technology and future applications. *Med. Laser Appl.* **2006**, *21*, 131–140. [CrossRef]
3. Salim, A.A.; Bidin, N. Pulse Q-switched Nd: YAG laser ablation grown cinnamon nanomorphologies: Influence of different liquid medium. *J. Mol. Struct.* **2017**, *1149*, 694–700. [CrossRef]
4. Marakis, G.; Pouli, P.; Zafiropulos, V.; Kalaitzaki, P.M. Comparative study on the application of the 1st and the 3rd harmonic of a Q-switched Nd: YAG laser system to clean black encrustation on marble. *J. Cult. Herit.* **2003**, *4*, 83–91. [CrossRef]
5. O'Mahony, M.J.; Simeonidou, D.; Hunter, D.K.; Tzanakaki, A. The application of optical packet switching in future communication networks. *IEEE Commun. Mag.* **2001**, *39*, 128–135.
6. Ma, Y.F.; Yu, X.; Li, X.D.; Fan, R.G.; Yu, G.H. Comparison on performance of passively Q-switched laser properties of continuous-grown composite $GdVO_4$/Nd:$GdVO_4$ and YVO_4/Nd:YVO_4 crystals under direct pumping. *Appl. Opt.* **2011**, *50*, 3854–3859. [CrossRef]
7. Ma, Y.F.; Zhang, S.C.; Ding, S.J.; Liu, X.X.; Yu, X.; Peng, F.; Zhang, Q.L. Passively Q-switched Nd:$GdLaNbO_4$ laser based on 2D $PdSe_2$ nanosheet. *Opt. Laser Technol.* **2020**, *124*, 105959. [CrossRef]
8. Schmidt, A.; Griebner, U.; Zhang, H.J.; Wang, J.Y.; Jiang, M.H.; Liu, J.H.; Petrov, V. Passive mode-locking of the Yb: CNGG laser. *Opt. Commun.* **2010**, *283*, 567–569. [CrossRef]
9. Zhang, H.J.; Zhao, S.Z.; Zhao, J.; Yang, K.J.; Li, G.Q.; Li, D.C.; Li, T.; Qiao, W.C.; Wang, Y.G. Generation of low repetition rate sub-nanosecond pulses in doubly QML Nd: $Lu_{0.5}Y_{0.5}VO_4$ and Nd:YVO_4 lasers with EO and transmission SSA. *Opt. Laser Technol.* **2015**, *69*, 39–43. [CrossRef]
10. Tang, W.; Zhao, J.; Yang, K.; Zhao, S.; Li, G.; Li, D.; Li, T.; Qiao, W. Experimental and Theoretical Investigation on Subnanosecond Pulse Characteristics from Doubly QML Nd: $Lu_{0.5}Y_{0.5}VO_4$ Green Laser. *IEEE J. Quantum Electron.* **2015**, *51*, 1700208.
11. Dong, L.; Huang, W.C.; Chu, H.W.; Li, Y.; Wang, Y.Z.; Zhao, S.Z.; Li, G.Q.; Zhang, H.; Li, D.C. Passively Q-switched near-infrared lasers with bismuthene quantum dots as the saturable absorber. *Opt. Laser Technol.* **2020**, *128*, 106219. [CrossRef]
12. Guo, B.; Xiao, Q.L.; Wang, S.H.; Zhang, H. 2D Layered Materials: Synthesis, Nonlinear Optical Properties, and Device Applications. *Laser Photonics Rev.* **2019**, *13*, 1800327. [CrossRef]

13. Chu, H.W.; Pan, Z.B.; Wang, X.; Zhao, S.Z.; Li, G.Q.; Cai, H.Q.; Li, D.C. Passively Q-switched Tm:Ca($Lu_{0.1}$Gd)AlO_4 laser at 2 µm with hematite nanosheets as the saturable absorber. *Opt. Exp.* **2020**, *28*, 16893–16899. [CrossRef]
14. Zhang, B.T.; Liu, J.; Wang, C.; Yang, K.J.; Lee, C.K.; Zhang, H.; He, J.L. Recent progress in 2D material-based saturable absorbers for all solid-state pulsed bulk lasers. *Laser Photonics Rev.* **2020**, *14*, 1900240. [CrossRef]
15. Chu, H.W.; Dong, L.; Pan, Z.B.; Ma, X.Y.; Zhao, S.Z.; Li, D.C. Passively Q-switched Tm:YAP laser with a zeolitic imidalate framework-67 saturable absorber operating at 3H4 → 3H5 transition. *Opt. Laser Technol.* **2022**, *147*, 107679. [CrossRef]
16. Zhong, H.; Yu, J.; Kuang, X.; Huang, K.; Yuan, S. Electronic and optical properties of monolayer tin diselenide: The effect of doping, magnetic field, and defects. *Phys. Rev. B* **2020**, *101*, 125430. [CrossRef]
17. Ding, Y.; Xiao, B.; Tang, G.; Hong, J. Transport Properties and High Thermopower of $SnSe_2$: A Full AbInitio Investigation. *J. Phys. Chem. C* **2017**, *121*, 225–236. [CrossRef]
18. Gonzalez, J.M.; Oleynik, I.I. Layer-dependent properties of SnS_2 and $SnSe_2$ two-dimensional materials. *Phys. Rev. B* **2016**, *94*, 125443. [CrossRef]
19. Huang, Y.; Xu, K.; Wang, Z.; Shifa, T.A.; Wang, Q.; Wang, F.; Jiang, C.; He, J. Designing the shape evolution of $SnSe_2$ nanosheets and their optoelectronic properties. *Nanoscale* **2015**, *7*, 17375–17380. [CrossRef]
20. Yu, P.; Yu, X.; Lu, W.; Lin, H.; Sun, L.; Du, K.; Liu, F.; Fu, W.; Zeng, Q.; Shen, Z.; et al. Fast photoresponse from 1T tin diselenide atomic layers. *Adv. Funct. Mater.* **2016**, *26*, 137–145. [CrossRef]
21. Cheng, C.; Li, Z.; Dong, N.; Wang, J.; Chen, F. Tin diselenide as a new saturable absorber for generation of laser pulses at 1 µm. *Opt. Exp.* **2017**, *25*, 6132–6140. [CrossRef] [PubMed]
22. Liu, X.Q.; Yang, Q.; Zuo, C.H.; Cao, Y.P.; Lun, X.L.; Wang, P.C.; Wang, X.Y. 2 µm passive Q-switched Tm:YAP laser with $SnSe_2$ absorber. *Opt. Eng.* **2018**, *57*, 126105. [CrossRef]
23. Wang, M.X.; Wang, Z.P.; Xu, X.G.; Duan, S.H.; Du, C.L. Tin diselenide-based saturable absorbers for eye-safe pulse lasers. *Nanotechnology* **2019**, *30*, 265703. [CrossRef] [PubMed]
24. Sun, R.Y.; Zhang, H.N.; Xu, N.N. High-power passively Q-switched Yb-doped fiber laser based on tin selenide as a saturable absorber. *Laser Phys.* **2018**, *28*, 085105. [CrossRef]
25. Hu, Q.; Li, M.; Li, P.; Liu, Z.; Cong, Z.; Chen, X. Dual-Wavelength Passively Mode-Locked Yb-Doped Fiber Laser Based on a $SnSe_2$-PVA Saturable Absorber. *IEEE Photonics J.* **2019**, *11*, 1503413. [CrossRef]
26. Sun, W.S.; Tang, W.J.; Li, X.Y.; Jiang, K.; Wang, J.; Xia, W. Stable soliton pulse generation from a $SnSe_2$-based mode-locked fiber laser. *Infrared Phys. Technol.* **2020**, *110*, 103451. [CrossRef]
27. Zhang, J.Y.; Sun, W.G.; Yuan, Y.; Zhang, H.K.; Tang, W.J.; Xia, W. Generation of rectangular pulses in ytterbium-doped fiber laser based on a $SnSe_2$ saturable absorber. *Infrared Phys. Technol.* **2022**, *120*, 103974. [CrossRef]
28. Li, T.; Zhao, S.; Zhuo, Z.; Yang, K.; Li, G.; Li, D. Dual-loss-modulated Q-switched and mode-locked YVO_4/Nd:YVO_4/KTP green laser with EO and Cr^{4+}:YAG saturable absorber. *Opt. Exp.* **2010**, *18*, 10315.
29. Tang, W.J.; Zhao, J.; Li, T.; Yang, K.J.; Zhao, S.Z.; Li, G.Q.; Li, D.C.; Qiao, W.C. High-peak-power mode-locking pulse generation in a dual-loss-modulated laser with BP-SA and EOM. *Opt. Lett.* **2017**, *42*, 4820–4823. [CrossRef]
30. Taube, A.; Łapińska, A.; Judek, J.; Zdrojek, M. Temperature dependence of Raman shifts in layered $ReSe_2$ and $SnSe_2$ semiconductor nanosheets. *Appl. Phys. Lett.* **2015**, *107*, 013105. [CrossRef]
31. Keller, U. Recent developments in compact ultrafast lasers. *Nature* **2003**, *424*, 831–838. [CrossRef]
32. Zhao, G.; Han, S.; Wang, A.; Wu, Y.; Zhao, M.; Wang, Z.; Hao, X. 'Chemical Weathering' Exfoliation of Atom-Thick Transition Metal Dichalcogenides and Their Ultrafast Saturable Absorption Properties. *Adv. Funct. Mater.* **2015**, *25*, 5292–5299. [CrossRef]
33. Wang, S.X.; Yu, H.H.; Zhang, H.J.; Wang, A.Z.; Zhao, M.W.; Chen, Y.X.; Mei, L.M.; Wang, J.Y. Broadband few-layer MoS_2 saturable absorbers. *Adv. Mater.* **2014**, *26*, 3538–3544. [CrossRef]
34. Wegner, U.; Meier, J.; Lederer, M.J. Compact picosecond mode-locked and cavity-dumped Nd:YVO_4 laser. *Opt. Express* **2009**, *17*, 23098–23103. [CrossRef]
35. Zhang, H.J.; Liu, J.H.; Wang, J.Y.; Wang, C.Q.; Zhu, L.; Shao, Z.S.; Meng, X.L.; Hu, X.B.; Chow, Y.T.; Jiang, M.H. Laser properties of different Nd-doped concentration Nd:YVO_4 laser crystals. *Opt. Lasers Eng.* **2002**, *38*, 527–536. [CrossRef]
36. *Digital Phosphor Oscilloscopes Quick Start User Manual*; Tektronix Inc.: Beaverton, OR, USA, 2013.
37. Yang, K.; Zhao, S.; He, J.; Zhang, B.; Zuo, C.; Li, G.; Li, D.; Li, M. Diode-pumped passively Q-switched and mode-locked Nd:$GdVO_4$ laser at 1.34 microm with V:YAG saturable absorber. *Opt. Express* **2008**, *16*, 20176–20185. [CrossRef]
38. Weller, D. Relating wideband DSO rise time to bandwidth: Lose the 0.35! *EDN* **2002**, *47*, 89–94.